JOURNAL OF COMPUTATIONAL PHYSICS 45, 307–344 (1982)

A Finite-Element Method for the 1-D Water Flooding Problem with Gravity

G. CHAVENT

INRIA, 78150 Le Chesnay, France

AND

G. SALZANO

CNR-IAC, Rome, Italy

Received May 6, 1980; revised October 28, 1981

The numerical simulation of the one-dimensional displacement of oil by water in a vertical porous slab is studied. The water saturation is governed by a *quasilinear diffusion–convection equation*. The diffusion term vanishes for the extreme values of the saturation. The *transport term* may be *nonmonotone* (for small or zero water injection rates in presence of gravity). Various boundary conditions are used: a *generalized Dirichlet condition* (for the pure transport case), and a condition taking into account the so-called "*well effect*" *on the production boundary* (for the case with capillary diffusion).

The above problem is solved using *discontinuous-finite elements together with mixed-finite elements*, following the ideas of Lesaint, Raviart and Thomas. Godunov's generalization of upstream weighting is also incorporated.

A computer code of this algorithm works satisfactorily under a wide range of experimental conditions, going from the pure diffusion case ($f \equiv 0$) to the pure transport case ($\alpha \equiv 0$). Results of various runs on idealized data as well as on laboratory data are shown.

1. INTRODUCTION

We shall discuss a numerical simulation of one-dimensional immiscible displacement in the presence of gravity. This type of displacement is currently performed in oil industry laboratories for the determination of the properties of core samples obtained during the drilling of wells. Such an experiment is shown in Fig. 1, where it clearly appears that gravity becomes the leading phenomenon for a sufficiently small water injection rate. The presence of gravity yields a nonmonotone-transport term in the saturation equation. The saturation equation contains a *degenerate nonlinear diffusion term due to capillary forces.*

The relative magnitude of those two terms varies from the *predominance of the transport term* (under field condition, or in high-speed laboratory displacements) to the *predominance of the capillary diffusion term* (in laboratory imbibition

0021-9991/82/030307-38$02.00/0

Copyright © 1982 by Academic Press, Inc.
All rights of reproduction in any form reserved.

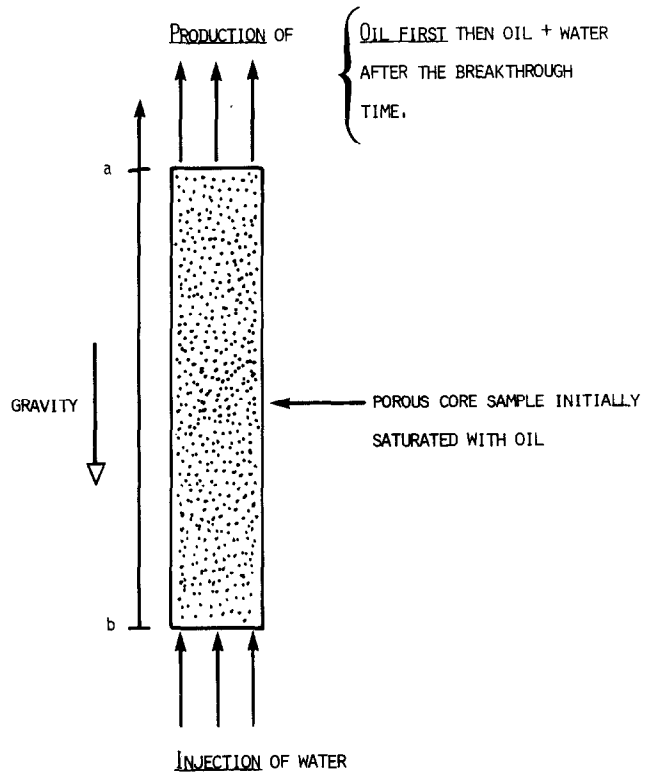

FIG. 1. A typical experiment of displacement of oil by water in a one-dimensional core sample.

experiments). The numerical algorithm should correctly solve the two limiting cases of the pure transport (or the Buckley–Leverett approximation, i.e., no capillary pressure) and of the pure diffusion (i.e., zero-fractional flow). *We present a method* using the recent results of Bardos–Leroux–Nedelec [1] for formulating the boundary conditions in the pure transport case, the finite-element methods of Raviart–Thomas [2] and Lesaint–Raviart [3] for approximating the diffusion and transport terms, and the technique of Godunov [4] adapted to finite elements for treating the case of nonmonotone first-order term. Moreover, we apply the boundary condition on the production end introduced by Chavent [5, 6]. This is the first time (to our knowledge) that all of the above techniques have been simultaneously employed for the simulation of immiscible displacement. The numerical technique is able to efficiently simulate displacements under the whole range of physically admissible conditions:

(i) large, slow, or zero water injection rate,

(ii) possibility of exchanging the injection and production end during the experiment,

(iii) presence or absence of capillary forces,

(iv) presence or absence of gravity, and

(v) various boundary conditions including those which take into account the so-called "well effect" at the production boundary.

We refer to the report of Salzano [7] for more details concerning the implementation of the techniques presented here. This has been used by Cohen [14, 17] for the construction of a code for automatic adjustment of relative-permeability curves. This analysis can be extended to the two-dimensional case (cf. the work of Jaffré [15, 16]).

2. Mathematical Formulation of the Immiscible Displacement Problem

Denote the space coordinate by x, and the reduced water saturation by $u(x, t)$, such that

$$0 \leqslant u(x, t) \leqslant 1. \tag{1}$$

Suppose that the *mean filtration velocity* $q(t)$ *is known.* This is the case for experiments with *imposed water injection* rates. In the case of experiments with *imposed pressure drop* ΔP, the mean filtration velocity $q(t)$ is given by

$$q(t) \int_a^b \frac{dx}{K\, d(u(x, t))} = \Delta P + q_1 \int_a^b \frac{\rho(u(x, t))}{K}\, dx \tag{2}$$

so that $q(t)$ has to be updated as u changes. This requires only minor changes in the solution of the equations, and we shall omit this case here.

The conservation law and the Darcy law for two-phase flow for incompressible fluids lead to the following equation for the saturation u (cf., e.g., [8, 9]):

$$\Phi \frac{\partial u}{\partial t} - \frac{\partial}{\partial x}\left(K \frac{\partial}{\partial x} \alpha(u)\right) + \frac{\partial}{\partial x}(b(u)\, q(t) + c(u) q_1) = 0. \tag{3}$$

The expressions of α, b, and c in terms of the relevant physical quantities are given in the Appendix. We shall discuss their typical shape and their physical effects.

$\alpha(u)$ is monotone increasing, with $\alpha'(0) = \alpha'(1) = 0$, and describes the *capillary diffusion,*

$b(u)$ is monotone increasing, with $b(0) = -1$ and $b(1) = +1$ and describes the *water transport caused by the mean filtration velocity* $q(t)$,

$c(u)$ is nonnegative, with $c(0) = c(1) = 0$, and describes the *water transport* caused by the gravity.

We define the function

$$f(u) = b(u)\, q(t) + c(u) q_1 \tag{4}$$

and the auxiliary variable

$$r = -K \frac{\partial}{\partial x} \alpha(u) \tag{5}$$

so that Eq. (3) may be rewritten as

$$\Phi \frac{\partial u}{\partial t} + \frac{\partial r}{\partial x} + \frac{\partial}{\partial x} [f(u)] = 0, \tag{6}$$

where f is monotone increasing or not depending upon the absence or presence of gravity. The water and oil filtration velocities ϕ_1 and ϕ_2 are given by

$$\phi_1(x, t) = q(t) + f(u) + r \tag{7}$$

$$\phi_2(x, t) = q(t) - f(u) - r. \tag{8}$$

The initial condition associated with (6) is

$$u(x, 0) = u_0(x), \qquad \forall x \in \Omega. \tag{9}$$

To specify the *boundary conditions* for (6) we have to *distinguish two cases.*

Case 1. $\alpha \equiv 0$, *i.e., pure transport equation.* Suppose we are given Dirichlet data $u_e(s)$ on the boundary $\Gamma = \{a, b\}$ of Ω. It is well known (cf. [18]) that the usual Dirichlet boundary condition

$$u(a, t) = u_e(a), \qquad u(b, t) = u_e(b)$$

cannot be satisfied for a first-order transport equation. For instance, if f is monotone increasing, the "good" condition is

$$u(a, t) = u_e(a), \qquad \text{no condition at} \quad x = b. \tag{10}$$

Conversely, if f is monotone decreasing, the "good" condition is

$$u(b, t) = u_e(b), \qquad \text{no condition at} \quad x = a. \tag{11}$$

When f is nonmonotone, the sign of $f'(u)$ on the boundary Γ of Ω is not a priori known. It depends on the value of the solution u, which, of course, is unknown. Hence, *it is not possible to know a priori the part of the boundary when the boundary value can be specified, and the part of the boundary where no condition can be imposed.* (Those two parts of the boundary do not necessarily coincide for nonmonotone f, with the water injection and production parts.) This problem has recently been solved by Bardos–Leroux–Nedelec [1], who imposed on the whole boundary Γ the condition

$$sg(u(s, t) - k)[f(u(s, t)) - f(k)]\nu_s \geqslant 0, \qquad \forall k \in I(u(s, t), u_e(s)), \quad \forall s \in \Gamma, \tag{12}$$

where

$$\begin{aligned} v_s &= +1 \quad \text{for} \quad s = b \\ &= -1 \quad \text{for} \quad s = a \end{aligned} \Big\} = \text{cosine of the "normal" to } \Omega \text{ with the } x \text{ axis.} \tag{13}$$

To understand the physical meaning of those boundary conditions, one can rewrite them as follows: at $x = a$, condition (12) is equivalent to the condition

$$\text{either} \quad u(a,t) = u_e(a),$$

$$\text{or} \quad u(a,t) \neq u_e(a) \quad \text{and} \quad \frac{f(u(a,t)) - f(k)}{u(a,t) - k} \leqslant 0$$

$$\forall k \in I(u_e(a); u(a,t)), \quad \forall t \in (0,T) \tag{12'}$$

and similarly at $x = b$. This means that, *on the boundary* Γ of Ω (cf. Fig. 2) either u is "*continuous*" (i.e., the Dirichlet condition is satisfied) or u is "*discontinuous*" *and* for every k in the range of discontinuity of u, the Rankine–Hugoniot direction of propagation of the discontinuity between u and k is outward from Ω.

Bardos *et al.* have shown in [1] that *system of equations* (6) (*with* $r \equiv 0$), (9) (12), or (12') *is well posed* in the sense that it admits a unique weak solution satisfying the entropy condition. Moreover, condition (12) or (12') is physically relevant in the following sense: the unique corresponding solution is the limit, as $\varepsilon \to 0$, of the solution u_ϵ of the parabolic equation obtained by adding an $\varepsilon \Delta u$ diffusion term and by imposing on Γ the usual Dirichlet condition $u = u_e$ (cf. [1] for the proof). This relevancy shall be confirmed numerically in Section 5 for the case of separation by gravity of two immiscible fluids in a vertical core sample.

In Section 3 we shall show that condition (12) or (12') is very easy to approximate numerically.

Case 2. $\alpha \not\equiv 0$, i.e., diffusion + transport equation. As in any difussion equation,

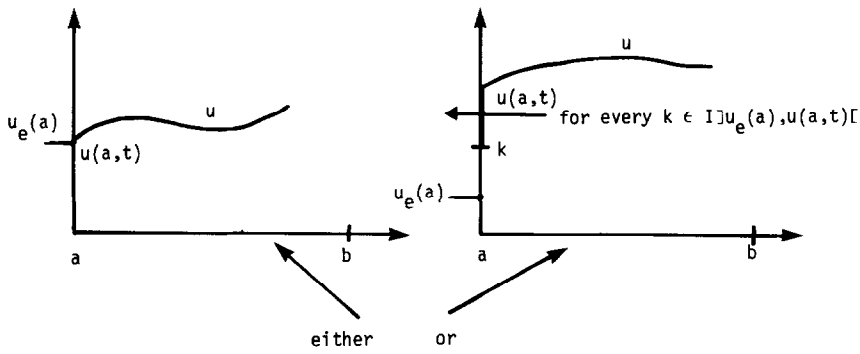

FIG. 2. Graphical representation of the Bardos–Leroux–Nedelec boundary condition for nonmonotone first order equations.

one can presumably take Dirichlet, Neumann, or unilateral boundary conditions for Eq. (3). The presence, however, of the capillary pressure

$$P_1 - P_2 = P_c(u), \tag{14}$$

where $P_c(u)$ satisfies

$$P_c'(u) > 0 \qquad \text{for} \quad u \in (0, 1),$$
$$P_c(u_p) = 0^*$$

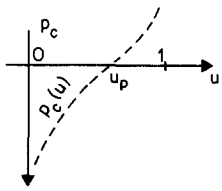

(which *cannot* be neglected as it is directly responsible for the presence of the diffusion term!) and the continuity requirement of both water and oil pressure P_1 and P_2 across the boundary prevent any simultaneous flow of oil and water across the boundary as long as $P_1 \neq P_2$, i.e., as long as $u \neq u_P$. So *in order to be physically admissible any solution* $u(x, t)$ *must satisfy the pressure continuity requirement*:

> simultaneous flow of oil and water may occur across the boundary if and only if the saturation $u = u_P$ at that point. PCR

At every point, denote $s \in \Gamma = \{a, b\}$:

$$\begin{aligned} u_s, \phi_{1s} &= \text{trace of water saturation and water filtration velocity,} \\ u_e(s)\, \phi_{1e}(s) &= \text{given values of the water saturation and filtration, when needed} \\ v_s = -1 \quad &\text{for} \quad s = a \\ = +1 \quad &\text{for} \quad s = b \end{aligned} \Big\} = \text{cosine of the "normal" to } \Gamma, \tag{15}$$

and *partition* Γ into Γ_- and Γ_+ *according to the sense of the mean-* (*oil and water*) *filtration velocity* $q(t)$ *across* Γ:

$$\begin{aligned} \Gamma_- &= \{s \in \Gamma \mid q(t) v_s \leqslant 0\} = \text{(overall) } \textit{injection boundary}, \\ \Gamma_+ &= \{s \in \Gamma \mid q(t) v_s > 0\} = \text{(overall) } \textit{production boundary}. \end{aligned} \tag{16}$$

The boundary conditions shall be:

* Generally, $u_p = 1$, if u is the wetting phase saturation.

On the injection boundary Γ_-

$$u_s = u_e(s) \qquad \text{(PCR satisfied if } u_e(s) = 1\text{)}, \tag{D}$$

$$\phi_{1s} = \phi_{1e}(s) \qquad \text{(PCR satisfied if } \phi_{1e}(s) = 0 \text{ (oil injection)} \text{ or if } \phi_{1e}(s) = 2q \text{ (water injection)}. \tag{N}$$

On the production boundary Γ_+

$$\text{as above,} \tag{D}$$

$$u_s \leqslant u_p, \qquad \phi_{1s}(s) v_s \geqslant 0, \quad (u_p - u_s)\phi_{1s} = 0 \quad \text{(always satisfies the PCR).} \tag{U}$$

Remark 1. From now on $q(t) > 0$ so that $\Gamma_- = \{a\}$ and $\Gamma_+ = \{b\}$. ∎

Remark 2. When $u_p = 1$, the unilateral boundary condition (U) means that, on the production boundary, the water accumulates until it reaches its maximum saturation value. This is the so-called "well effect" described in the petroleum engineering literature. ∎

Remark 3. Equations (3) and (9), together with one of the above boundary conditions meeting the PCR, satisfy a *maximum principle*. This ensures that

$$0 \leqslant u(x, t) \leqslant 1 \tag{17}$$

for an adequate continuation of the function $f(u)$ for values of u outside of the $[0, 1]$ interval. It is then possible to show existence and in some cases uniqueness of a solution of those equations. We refer to Chavent [5, 9, 10] and Gagneux [11] for the mathematical study of the corresponding variational equalities and inequalities. ∎

3. Approximation of Case 1: Transport Equation

Consider the approximation of Eq. (6) (with $r \equiv 0$) together with the Dirichlet boundary conditions (12), (13), and initial condition (9). Discretize the space domain $\Omega = (a, b)$ into I intervals (x_i, x_{i+1}), $i = 1, 2, \ldots, I$ and the time domain $]0, T[$ into N intervals $[t^n, t^{n+1}]$ $n = 1, 2, \ldots, N$ of length Δt. Let k be a given nonnegative integer (we shall use $k = 0$ and $k = 1$ in the numerical examples), and define:

$$V_h = \{v_h \in L^2(\Omega) \mid v_h|_{(x_i, x_{i+1})} \in \mathscr{P}^k, \qquad i = 1, 2, \ldots, I\}, \tag{18}$$

$$u_{0h} \in V_h, \qquad \text{an approximation to the initial function } u_0. \tag{19}$$

Let $(u_h^n \in V_h,\ n = 1, \ldots, N+1)$ be the desired approximation of $u(x, t)$ (cf. Fig. 3). At

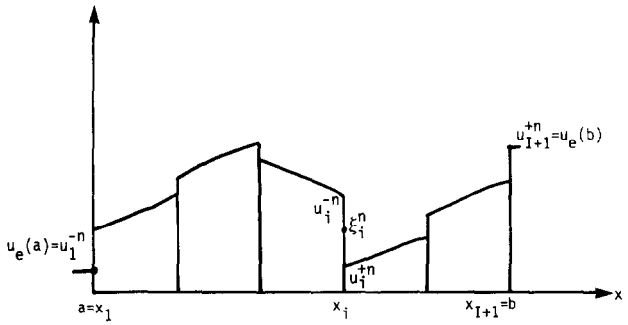

FIG. 3. The function u_h^n approximating $u(\cdot, t^n)$ in the space V_h, and the boundary data $u_e(a)$ and $u_e(b)$.

every point of discontinuity x_i of u_h^n, $i = 1,..., I+1$ (hence, including a and b) define the Godunov value ξ_i^n (see Godunov [4], Leroux [12]) by

$$\begin{aligned} &u_i^{+n} = u_h^n(x_i + 0, t^n), \qquad i = 1,..., I, \qquad u_{I+1}^{+n} = u_e(b), \\ &u_1^{-n} = u_e(a), \qquad u_i^{-n} = u_h^n(x_i - 0, t^n), \qquad i = 2,..., I+1, \\ &\quad sg(u_i^{+n} - u_i^{-n}) f(\xi_i^n) \leqslant sg(u_i^{+n} - u_i^{-n}) f(k), \\ &\quad \forall k \in I(u_i^{-n}, u_i^{+n}), \qquad \forall i = 1, 2,..., I+1. \end{aligned} \tag{20}$$

Remark 4. As only $f(\xi_i)$ appears in the computations, the possible nonuniqueness of ξ_i defined by (20) does not cause a problem. This practical determination of the ξ_i^n's is easy, e.g., by exploration technique if f is continuous and piecewise linear. ∎

Remark 5. Let us denote by $\hat{u}^n(x, t)$, $x \in \mathbb{R}$, $t \geqslant t^n$, the exact solution of Eq. (6) (with $r \equiv 0$) on $\mathbb{R}$ with initial condition

$$\begin{aligned} \hat{u}^n(x, t^n) &= u_e(a), \qquad \text{for} \quad x \leqslant a, \\ &= u_h^n, \qquad \text{for} \quad a < x < b, \\ &= u_e(b), \qquad \text{for} \quad x \geqslant b. \end{aligned}$$

Then one can check, using the method of characteristics for the calculation of $\hat{u}^n(x, t)$, that

$$\begin{aligned} &\text{if } \xi_i^n \text{ is uniquely defined by (20), then } \hat{u}^n(\cdot, t^n + 0) \text{ is continuous at } x = x_i, \\ &\text{and, then } \xi_i^n = \hat{u}^n(x_i, t^n + 0), \\ &\text{if Eq. (20) admits } p \text{ solutions } \xi_{i1}^n \leqslant \xi_{i2}^n \leqslant \cdots \leqslant \xi_{ip}^n, \text{ then } \hat{u}^n(\cdot, t^n + 0) \text{ is} \\ &\text{discontinuous at } x = x_i \text{ and jumps from } \xi_{i1}^n \text{ to } \xi_{ip}^n. \end{aligned} \tag{21}$$

Hence, the Godunov value ξ_i^n simply represents the value of the solution that would

occur at x_i at time $t^n + 0$ if the equation were exactly solved starting with the initial value u_h^n.

If f is monotone increasing (resp. decreasing) on $I(u_i^{-n}, u_i^{+n})$, then ξ_i^n coincides with the usual upstream value u_i^{-n} (resp. u_i^{+n}). ∎

We define the sequence $\{u_h^n \in V_h,\ n = 1, 2,..., N+1\}$ *by*

$$u_h^1 = u_{0h} \tag{22}$$

$$\int_{x_i}^{x_{i+1}} \Phi \frac{u_h^{n+1} - u_h^n}{\Delta t} v\, dx + \int_{x_i}^{x_{i+1}} \frac{\partial f(u_h^n)}{\partial x} v\, dx + (f(u_i^{+n}) - f(\xi_i^n))\, v(x_i)$$
$$- (f(u_{i+1}^{-n}) - f(\xi_{i+1}^n))\, v(x_{i+1}) = 0, \tag{23}$$
$$\forall v \in \mathscr{P}^k, \quad \forall i = 1,..., I, \qquad \forall n = 1,..., N,$$

where the $\xi_i^n i = 1,..., I+1$, $n = 1,..., N$, are computed from u_h^n and the boundary values $u_e(a)$, $u_e(b)$ by (20).

Remark 6. Boundary conditions (12) and (13) are taken into account very simply in scheme (22), (23) by the fact that the Godunov values ξ_1 and ξ_{N+1} at $x_1 = a$ and $x_{N+1} = b$ are calculated using the "Dirichlet data" $u_e(a)$ and $u_e(b)$ as "exterior values" (cf. (20)). For the continuous case, if we define Godunov values $\xi_a(t)$ and $\xi_b(t)$, $t \in [0, T]$ similarly to (20), then boundary conditions (12) and (13) can be rewritten as

$$f(u(a+0, t)) = f(\xi_a(t)), \qquad \forall t \in [0, T], \tag{12''}$$

$$f(u(b-0, t)) = f(\xi_b(t)), \qquad \forall t \in [0, T], \tag{13''}$$

which implies that the solution *has to meet continuously* with the Godunov value ξ on the boundary when this values is unique. This property is only approximately satisfied by the solution u_h^n (generally, $u_1^{+n} \neq \xi_1^n$ and $u_{I+1}^{-n} \neq \xi_{I+1}^n$). ∎

Remark 7. The proper discretization for the water and oil filtration velocities ϕ_1 and ϕ_2 defined in (7) and (8) is

$$\phi_{1h}(x_i, t^n) = q(t^n) + f(\xi_i^n), \qquad i = 1, 2,..., I+1, \quad n = 1, 2,..., N+1, \tag{7'}$$

$$\phi_{2h}(x_i, t^n) = q(t^n) - f(\xi_i^n), \qquad i = 1, 2,..., I+1, \quad n = 1, 1,..., N+1, \tag{8'}$$

and one can easily check that scheme (22), (23), together with (7') and (8'), satisfies the mass balance exactly. ∎

An alternative formulation of (23) is obtained by integrating by parts the term containing $\partial f/\partial x$

$$\int_{x_i}^{x_{i+1}} \Phi \frac{u_h^{n+1} - u_h^n}{\Delta t} v\, dx - \int_{x_i}^{x_{i+1}} f(u_h^n) \frac{\partial v}{\partial x} dx + f(\xi_{i+1}^n)\, v(x_{i+1}) - f(\xi_i^n)\, v(x_i) = 0, \tag{23'}$$
$$\forall v \in \mathscr{P}^k, \quad \forall i = 1, 2,..., I, \quad \forall n = 1, 2,..., N.$$

We now examine, for a regular space discretization of step size h, the different schemes obtained by choosing $k=0$ and $k=1$ in definition (18) of V_h (all those schemes are explicit (as Scheme (22), (23) is) and hence, require a Courant–Friedrichs–Lewy type condition in order to ensure stability).

$k=0$: *Finite Differences*

$$V_h = \textit{space of piecewise-constant functions on each interval.} \tag{24}$$

Define

$$u^n_{i+1/2} = \text{(constant) value of } u_h \text{ on } (x_i, x_{i+1}), \tag{25}$$

then scheme (22), (23) *reduces to*

$$u^1_{i+1/2} = u_{0h,i+1/2}, \qquad i = 1,\ldots, I, \tag{26}$$

$$\phi \frac{u^{n+1}_{i+1/2} - u^n_{i+1/2}}{\Delta t} + \frac{f(\xi^n_{i+1}) - f(\xi^n_i)}{h} = 0, \qquad i = 1,\ldots, I, \quad n = 1,\ldots, N \tag{27}$$

with ξ_i, $i = 1, 2,\ldots, I+1$ defined by (20).

This is the Godunov scheme for finite differences, which has been extensively studied by Leroux in his thesis [12]. Leroux proves, under the Courant–Friedrichs–Lewy stability condition, the convergence of the u^n_h, defined by (26) and (27), to the unique solution u of (6) with $r=0$ and (9), (12), and (13) satisfying the entropy condition.

This scheme is known to satisfy a discrete maximum principle: if the initial and boundary data u_{0h}, $u_e(a)$, $u_e(b)$ belong to $[0, 1]$, then u_h does, too. There is no need to numerically define the function $f(u)$ for values of u which do not belong to $[0, 1]$, as the computer program never requires such an evaluation.

Finally, notice that, using Remark 5, the above scheme for monotone functions f reduces to the usual upstream weighting finite-difference scheme.

$k=1$: *Linear-Discontinuous Finite Elements*

Now

$$V_h = \textit{space of piecewise-linear functions on each interval.} \tag{28}$$

Equations (23) and (23′) give, using the Simpson formula for the calculation of the integrals in (23) bis, with the notation of Fig. 3

$$\Phi \frac{u^{+n+1}_i - u^{+n}_i}{\Delta t} + \frac{f(u^{+n}_i) + 4f(u^n_{i+(1/2)}) + f(u^{-n}_{i+1}) - 2f(\xi^n_{i+1}) - 4f(\xi^n_i)}{h} = 0 \tag{29}$$

$$\Phi \frac{u^{-n+1}_{i+1} - u^{-n}_{i+1}}{\Delta t} + \frac{-f(u^{+n}_i) - 4f(u^n_{i+(1/2)}) - f(u^{-n}_{i+1}) + 4f(\xi^n_{i+1}) + 2f(\xi^n_i)}{h} = 0 \tag{30}$$

with ξ^n_i defined by (20) and $u_{i+1/2} = \frac{1}{2}(u^+_i + u^-_{i+1})$.

In the linear case ($f(u)=u$) this scheme reduces to that of Lesaint [3], who has proven that it is convergent and of order two if u is regular. If $\Delta t/h \to 0$ scheme (29), (30) tends to one of the second-order schemes proposed by Van Leer [13].

In the nonlinear case convergence of u_h to the minimum entropy solution has not been proven. However, the construction of the scheme suggests that it will be well behaved on that point. This is confirmed by the numerical results (cf. Section 5). As scheme (29), (30) does not satisfy a maximum principle, there is no guarantee that u_h^n will remain between 0 and 1. Generally, it does not. *So one has to define the function $f(u)$ for values of u smaller than zero and greater than one.* The choice of the continuation may significantly influence the efficiency of the scheme. For instance, for displacements experiments ($q>0$) *the following continuation* works for $\lambda > 0$ large enough with respect to $f(1)-f(0)=2q(t)$

$$f(u)=f(1)+\lambda(u-1), \qquad \text{for} \quad u>1, \tag{31}$$

$$f(u)=f(0), \qquad \text{for} \quad u<0. \tag{32}$$

(The same continuation with $\lambda = 0$ does not work, as the portion of the curves above $u=1$ has a speed equal to zero and, hence, never disappears.)

4. Approximation of Case 2: Diffusion + Transport Equation

Consider the approximation of the full equation (6) together with (5), initial condition (9), and Dirichlet, Neumann, or unilateral boundary conditions. *In this case $u(\cdot, t)$ is continuous for almost every t*, so it has a trace on $\Gamma = \{a, b\}$. We want to determine

$$(u_h^n \in V_h,\ n=1, 2,..., N+1) = \text{approximation of } u \text{ on } (a,b)\times[0,T], \tag{33}$$

$$(u_s^n \in R,\ s\in\Gamma,\ n=1, 2,..., N+1) = \text{approximation of the trace of } u \text{ on } \Gamma\times[0,T] \tag{34}$$

$$(r_h^n \in Q_h,\ n=1, 2,..., N+1) = \text{approximation of } r=-K\frac{\partial}{\partial x}\alpha(u) \text{ on } (a,b)\times[0,T], \tag{35}$$

where Q_h is defined by (*mixed*-finite elements, cf. Raviart–Thomas [2])

$$Q_h = \{s_h \in \mathscr{C}^0([a,b]) \mid s_h|(x_i, x_{i+1}) \in \mathscr{P}^{k+1},\ i=1, 2,..., I\}. \tag{36}$$

The use of mixed-finite elements (i.e., the use of a supplementary unknown r_k^n) for the discretization of the diffusion term *follows* naturally from the *choice of a discontinuous approximation u_h^n made for u*, which was made according to Lesaint's *ideas for a proper discretization of the transport term.*

For the determination of $(u_h^n, u_s^n, r_h^n,\ n=1, 2,..., N+1)$ we use the following: Equation inside $(a,b)\times[0,T]$. Equation (6) is approximated, as in Case 1 of the

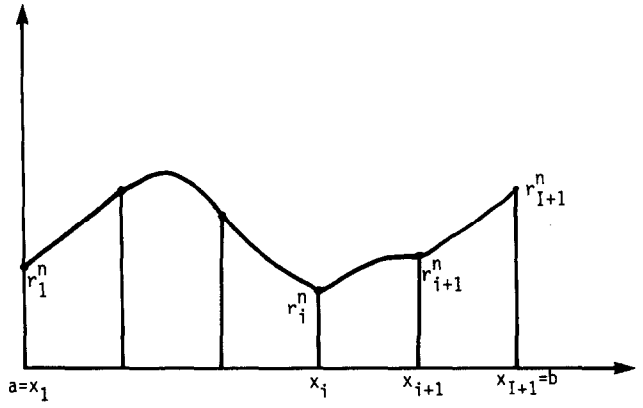

FIG. 4. The function r_h^n approximating $u(\cdot, t^n)$ in the space Q_h.

pure transport equation, by Eq. (23) or (23′) with an additional term for the approximation of the diffusion term $\partial r/\partial x$. This yields

$$\int_{x_i}^{x_{i+1}} \Phi \frac{u_h^{n+1}-u_h^n}{\Delta t} v + \int_{x_i}^{x_{i+1}} \frac{\partial r_h}{\partial t} v - \int_{x_i}^{x_{i+1}} f(u_h^n) \frac{\partial v}{\partial x} dx + f(\xi_{i+1}^n)\, v(x_{i+1}) - f(\xi_i^n)\, v(x_i) = 0, \qquad \forall v \in \mathscr{P}^k, \quad \forall i = 1, 2, \ldots, I, \quad \forall n = 1, 2, \ldots, N, \tag{37}$$

where the ξ_i^n are given by (20) with the following changes in the definition of u_1^{-n} and u_{I+1}^{+n}:

$$\begin{aligned} u_1^{-n} &= u_a^n \qquad \text{(instead of } u_e(a)\text{)}, \\ u_{I+1}^{+n} &= u_b^n \qquad \text{(instead of } u_e(b)\text{)}. \end{aligned} \tag{38}$$

Equation (5) is approximated by

$$\int_a^b r_h^n s_h\, dx = \int_a^b \alpha(u_h^n) \frac{\partial s_h}{\partial x} + \alpha(u_a^n)\, s_h(a) - \alpha(u_b^n)\, s_h(b), \qquad \forall s_h \in Q_h, \quad \forall n = 1, 2, \ldots, N+1. \tag{39}$$

The water filtration velocity ϕ_1 at point x_i is approximated by

$$\phi_{1h}(x_i, t^n) = q(t^n) + f(\xi_i^n) + r_i^n, \qquad i = 1, 2, \ldots, I+1, \quad n = 1, \ldots, N+1. \tag{40}$$

Initial conditions (as for Case 1)

$$u_h^1 = u_{0h}. \tag{22}$$

Boundary conditions. We have seen in Section 2 that one can have at point s

on the boundary $\Gamma = \{a, b\}$ of Ω a Dirichlet condition (D) or Neumann condition (N) or a unilateral condition (U).

For numerical calculations, the *unilateral* condition (U) reduces either to a Neumann *no-water-flow condition* (before the breakthrough, i.e., *as long as the resulting boundary saturation* u_s^n *is smaller than* u_p) or *to a Dirichlet maximum water saturation condition* (after the breakthrough, i.e., as long as the resulting water flow ϕ_{1s_h} is directed *out of* Ω).

So it is only necessary to define, for any $s \in \Gamma = \{a, b\}$, the *discretization of the Dirichlet and Neumann conditions*

$$\forall s \in \Gamma = \{a, b\}, \quad \forall n = 1, 2, \ldots, N+1, \text{ either: } u_s^n = u_e(s), \tag{41D$_h$}$$

$$\text{or: } \phi_{1s_h}^n = q(t^n) + f(\xi_s^n) + r_h^n(s) = \phi_{1e}(s). \tag{41N$_h$}$$

Equations (20), (22), (37)–(39) and (41) completely determine the set of unknown (33)–(35).

Suppose that u_h^n, u_s^n, r_h^n are known.

Step 1. Calculate the Godunov value ξ_i^n, $i = 1, \ldots, I+1$ using Eqs. (20) and (38).

Step 2. Calculate u_h^{n+1} using explicit equation (37).

Step 3. Using Eq. (39) and boundary conditions (41) all written at time $n+1$, calculate u_s^{n+1} and r_h^{n+1}:

For the Dirichlet boundary condition. u_s^{n+1} is given directly by (D$_h$) of (41) and then Eq. (39) gives r_h^{n+1} through the resolution of linear system (possibly diagonal in the 1-D case with numerical quadrature formulae).

For the Neumann boundary condition. Here, the situation is more complicated. In Eq. (41N$_h$) both $f(\xi_s^n)$ and $r_h^n(s)$ depend, in a nonlinear way, on u_s^n (the first one through (20) and (38), the second through (39)). We shall check directly on the equation obtained for $k = 0$, 1 that those equations uniquely determine u_s^{n+1} and r_h^{n+1}.

We develop Eqs. (37)–(39) and (41) for $k = 0$ and $k = 1$.

$k = 0$ (Finite Differences)

Then r_h is continuous and piecewise linear on each interval $]x_i, x_{i+1}[$, $i = 1, \ldots, I$. Hence, the free variables for r_h are $r_i = r_h(x_i)$, $i = 1, 2, \ldots, I+1$. Equation (37) gives

$$\Phi \frac{u_{i+1/2}^{n+1} - u_{i+1/2}^n}{\Delta t} + \frac{r_{i+1}^n - r_i^n}{h} + \frac{f(\xi_{i+1}^n) - f(\xi_i^n)}{h} = 0,$$
$$i = 1, \ldots, I, \quad n = 1, \ldots, N, \tag{42}$$

and Eq. (39) becomes, in matrix form,

$$M \begin{bmatrix} r_1^n \\ \vdots \\ r_{I+1}^n \end{bmatrix} = \frac{1}{h} \begin{bmatrix} \alpha(u_a^n) - \alpha(u_{1/2}^n) \\ \alpha(u_{1/2}^n) - \alpha(u_{3/2}^n) \\ \vdots \\ \alpha(u_{I+1/2}^n) - \alpha(u_b^n) \end{bmatrix}, \tag{43}$$

where the matrix M is given by

$$M = \begin{bmatrix} \frac{1}{3} & \frac{1}{6} & & 0 \\ \frac{1}{6} & \frac{2}{3} & & \\ & & & \\ & 0 & \frac{2}{3} & \frac{1}{6} \\ & & \frac{1}{6} & \frac{1}{3} \end{bmatrix} \tag{44}$$

if the integrals in (39) are calculated exactly.

$$M = \begin{bmatrix} \frac{1}{2} & & & 0 \\ & 1 & & \\ & & & \\ & 0 & 1 & \\ & & & \frac{1}{2} \end{bmatrix} \tag{45}$$

if the integrals in (39) are calculated using the *trapezoidal rule*. In the latter case, Eqs. (42) and (43) give the usual three-point approximation of the Laplacian.

Suppose now that M *is given by* (45) *and examine boundary condition* (41):

Dirichlet condition D_h

$$u_s^n = u_e(s), \qquad s \in \Gamma = \{a, b\} \tag{46}$$

and, hence, the right-hand side of (43) is known completely.

Neumann condition N_h. From definition (20) of ξ_i^n note that $f(\xi_i^n)$ *is a function* of the left- and right-hand values u_i^{-n} and u_i^{+n} of u at x_i

$$f(\xi_i^n) = \theta(u_i^{-n}, u_i^{+n}). \tag{47}$$

It is easy to check from (20) that (cf. Fig. 5)

$$\begin{aligned} &\theta \text{ is an increasing function of its first argument and} \\ &\quad \text{a decreasing function of its second argument.} \end{aligned} \tag{48}$$

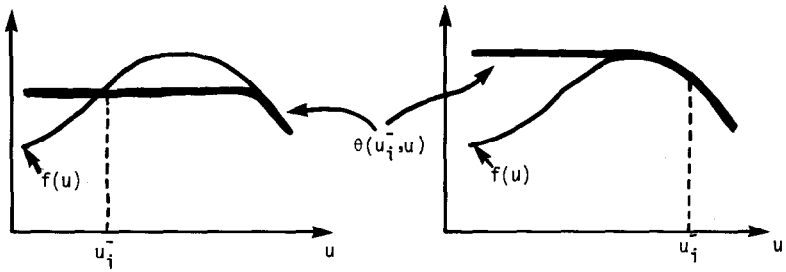

FIG. 5. The function $\theta(u_i^-, \cdot)$ for two values of u_i^- and function f showing only one maximum.

Condition ($41N_h$) can be rewritten, using (47), (38), and the first and last equation in (43) as

$$\theta(u_a^n, u_1^{+n}) + (2/h)\,\alpha(u_a^n) = \phi_{1e}(a) - q(t^n) + (2/h)\,\alpha(u_{1/2}^n), \qquad \text{for} \quad s = a, \tag{49}$$

$$\theta(u_{I+1}^{-n}, u_b^n) - (2/h)\,\alpha(u_b^n) = \phi_{1e}(b) - q(t^n) - (2/h)\,\alpha(u_{I+1/2}^n), \qquad \text{for} \quad s = b. \tag{50}$$

As α is strictly monotone increasing, Eqs. (49) and (50) uniquely determine u_a^n and u_b^n once u_h^n is known. This is the case during Step 3 of the above step-by-step solution.

The determination of u_a^n requires one inversion of the nonlinear function $\theta(\cdot, u_1^{+n}) + (2/h)\,\alpha(\cdot)$. As the functions α and f are generally given point by point, and linearly interpolated between thoses points, the inversion is done by exploration techniques.

$k = 1$ *(Linear-Discontinuous Finite Elements)*

r_h is continuous and piecewise quadratic. The corresponding free variables are $r_i = r_h(x_i)$, $i = 1, 2, \ldots, I+1$ and $r_{i+1/2} = r_h((x_i + x_{i+1})/2)$, $i = 1, 2, \ldots, I$. (As the integrals in (37) and (39) involving the functions f and α usually cannot be calculated exactly with ease, one has to use quadrature formulae). The following choices have been tested by Cohen [14]:

(i) Trapezoidal rule in (37) and in the right-hand side of (39), Simpson rule in (39).

(ii) Trapezoidal rule in (37), Simpson rule in (39).

(iii) Simpson rule in both (37) and (39).

As choice (iii) has been shown to give the sharpest front, *we shall develop* (37) *and* (39) *for* $k = 1$ *only with choice* (iii) *for the quadrature formulae.* Equation (37) becomes:

$$\begin{aligned} &\text{Eq. (29)} \quad \text{with} \quad (-3r_i^n + 4r_{i+1/2}^n - r_{i+1}^n)/h \quad \text{added to the left-hand side, and} \\ &\text{Eq. (30)} \quad \text{with} \quad (r_i^n - 4r_{i+1/2}^n + 3r_{i+1}^n)/h \quad \text{added to the left hand side,} \end{aligned} \tag{51}$$

and Eq. (39) becomes (with the notation $\alpha_i^{+n} = \alpha(u_i^{+n})$, etc.)

$$
\begin{aligned}
r_1^n &= (1/h)[6\alpha(u_a^n) - 3\alpha_1^{+n} - 4\alpha_{3/2}^n + \alpha_2^{-n}], \\
r_i^n &= (1/2h)[-\alpha_{i-1}^{+n} + 4\alpha_{i-1/2}^n + 3\alpha_i^{-n} - 3\alpha_i^{+n} - 4\alpha_{i+1/2}^n + \alpha_{i+1}^{-n}], \qquad i = 2,..., I, \\
r_{i+1/2} &= (1/h)[\alpha_i^{+n} - \alpha_{i+1}^{-n}], \qquad i = 1, 2,..., I, \\
r_{I+1}^n &= (1/h)[-\alpha_I^{+n} + 4\alpha_{I+1/2}^n + 3\alpha_{I+1}^{-n} - 6\alpha(u_b^n)].
\end{aligned} \tag{52}
$$

We now examine the boundary conditions.

The Dirichlet condition (D_h) becomes (46) (as for $k = 0$) which determines the values of $\alpha(u_a^n)$ and/or $\alpha(u_b^n)$ in the right-hand side of (52).

The Neumann condition (N_h) becomes, with notation (47)

$$\theta(u_a^n, u_1^{+n}) + (6/h)\,\alpha(u_a^n) = \phi_{1e}(a) - q(t^n) + (1/h)[3\alpha_1^{+n} + 4\alpha_{3/2}^n - \alpha_2^{-n}], \tag{53}$$

$$\theta(u_{I+1}^{-n}, u_b^n) - (6/h)\,\alpha(u_b^n) = \phi_{1e}(b) - q(t^n) + (1/h)[\alpha_I^{+n} - 4\alpha_{I+1/2}^n - 3\alpha_{I+1}^{-n}] \tag{54}$$

which uniquely determines u_a^n and u_b^n when u_h^n is known.

5. The Numerical Results

1. *The Data*

Our numerical tests have been performed using three sets of data: *one set of idealized data* (allowing comparison with exact solutions in the pure transport case), and *two sets of laboratory data*[1] (including transport and imbibition experiments with and without gravity). Hereinafter u denotes the injected fluid saturation.

The Set of Idealized Data (ID)

The data common to the various runs are

$$
\begin{gathered}
a = 0, \qquad b = 1, \qquad K = \Phi = 1, \qquad U_{\min} = 0, \qquad U_{\max} = 1, \\
f(u) = u(1-u) \quad \text{(strongly nonmonotone!)} \\
u_0(x) = (b-x)/(b-a), \qquad \forall x \in [a, b]
\end{gathered} \tag{55}
$$

and the characteristics that vary from one run to the other are:

(i) the diffusion function $\alpha(u)$, which is either identically zero (for pure transport runs) or is taken linear: $\alpha(u) = 0.1 \times u$ (for runs with diffusion),

(ii) the boundary conditions which shall be specified in each run, and

(iii) the type of approximation ($k = 0$) or ($k = 1$) and the space and time step.

[1] Data considerately supplied by the Société Nationale Elf Aquitaine.

Remark 8. This set of idealized data models the action of gravity, (with $g = 1$!) in a vertical core sample ($\cos\gamma = +1$) on two immiscible fluids maintained under hydrostatic pressure equilibrium (i.e., $q(t) \equiv 0$) and having the following idealized characteristics (one can think of fluid 1 (resp. fluid 2) as being water (resp. oil).

$$\mu_1 = \mu_2 = 1, \qquad \rho_1 - \rho_2 = 1,$$

$$k_{1r}(u) = u, \qquad k_{2r}(u) = 1 - u \qquad \text{(straight-line relative permeabilities)},$$

$$\frac{dp_c}{du}(u) = \text{either } 0 \quad \text{or} \quad \frac{1}{u(1-u)}.$$

The First Set of Laboratory Data (LD1)

In order to have a strong influence of gravity, we have first chosen gas as fluid 1 (injected fluid) and oil as fluid 2 (resident fluid). The pressure drop across the sample is supposed small enough so that gas can be taken as incompressible. The data common to all runs are (u = gas saturation)

$$a = 0 \text{ cm}, \qquad b = 38 \text{ cm}, \qquad \sigma = 20 \text{ cm}^2,$$

$$K = 83 \text{ md}, \qquad \phi = 0.1, \qquad U_{\min} = 0, \qquad U_{\max} = 0.65,$$

$$g = 980 \text{ cm/s/s},$$

$$\mu_1 = 0.0128 \times 10^{-2} \text{ poises}, \qquad \mu_2 = 0.208 \times 10^{-2} \text{ poises}, \tag{58}$$

$$\rho_1 = 0.0183 \text{ g/cm}^3, \qquad \rho_2 = 0.6225 \text{ g/cm}^3,$$

$k_{1r}(u)$, $k_{2r}(u)$ and $p_c(u)$ are the continuous piecewise linear functions of u shown in Fig. 6. (The gas/oil mobility ratio is 3.64.)

We see from Fig. 6 that the capillary pressure vanishes for the gas saturation $u_p = U_{\min}$, so that the *unilateral condition reduces to the simple Dirichlet condition* $u = U_{\min}$. The characteristics that may change from one run to another are:

(ii) *the shape of the transport function* $f(u)$, which depends (cf. (4)) on the mean (gas + oil) *filtration velocity* q and on the *cosine of the angle* γ of the x axis with the vertical direction oriented downward as shown in Fig. 7,

(ii) *the diffusion function* $a(u)$ which is either that of Fig. 6 or taken equal to zero,

(iii) *the boundary conditions*, which are choosen according to Section 2, and shall be specified for each run, and

(iv) *the initial condition* which can be either

$$u_0(x) = 0 \qquad \text{or} \qquad u_0(x) = 0.65 * (b - x)/(b - a). \tag{59}$$

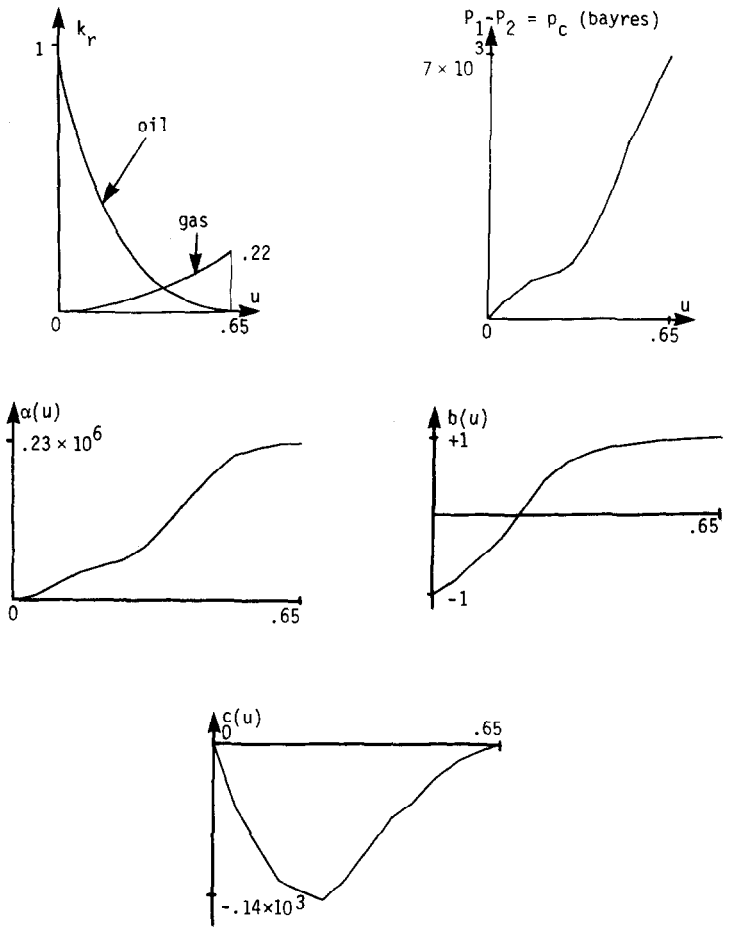

FIG. 6. The relative permeability and capillary pressure curves for the first set of laboratory data (gas and oil) and the corresponding function $\alpha(u)$, $b(u)$, and $c(u)$ used in the numerical calculations.

The Second Set of Laboratory Data (LD2)

To simulate imbibition experiments and to illustrate the effects of the unilateral boundary condition in the case where it does not reduce to a Dirichlet condition we use a second set of laboratory data corresponding to the displacement of oil (fluid 2) by water (fluid 1).

The data common to all runs are (u = water saturation)

$a = 0$ cm, $\sigma = 45$ cm^2,

$K = 23.1$ md, $\phi = 0.328$, $U_{\min} = 0.24$, $U_{\max} = 0.76$,

$g = 980$ cm/s/s,

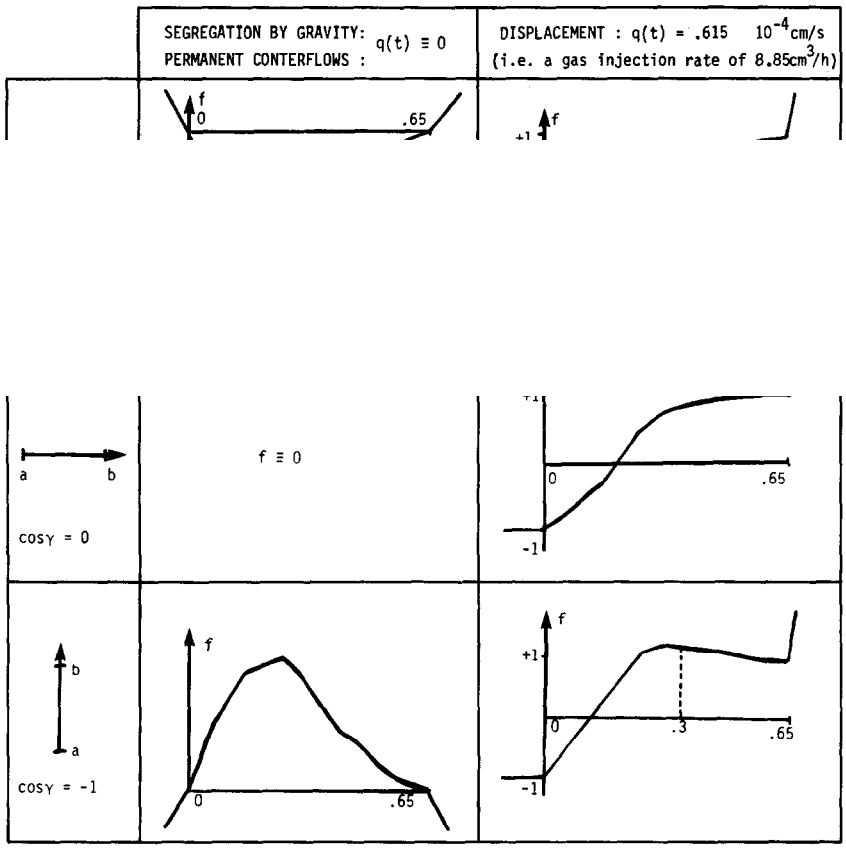

FIG. 7. The shape of the function $f(u)$ and the chosen continuations out of the (0, 0.65) interval for different values of q and $\cos\gamma$ (first set of laboratory data: gas and oil).

$$\mu_1 = 0.46 \times 10^{-2} \text{ poises}, \qquad \mu_2 = 1.92 \times 10^{-2} \text{ poises},$$

$$\rho_1 = 1.2 \text{ g/cm}^3, \qquad \rho_2 = 0.5 \text{ g/cm}^3,$$

$k_{1r}(u)$, $k_{2r}(u)$, and $p_c(u)$ as shown on Fig. 8 (the water/oil mobility ratio is 0.58). (60)

The corresponding functions $a(u)$, $b(u)$, and $c(u)$ are similar to those of Fig. 6 (but with $c \geqslant 0$, instead of $c \leqslant 0$) and are not shown here. The capillary pressure vanishes for $u = U_{\max}$, so that the unilateral boundary condition shall cause an accumulation of water against the production end. The characteristics that shall vary from one run to the other are:

(i) the magnitude of the capillary pressure (cf. Fig. 8),

(ii) the length of the sample: $b = 15.5$ cm for imbibition experiments and $b = 31$ cm for displacement experiments,

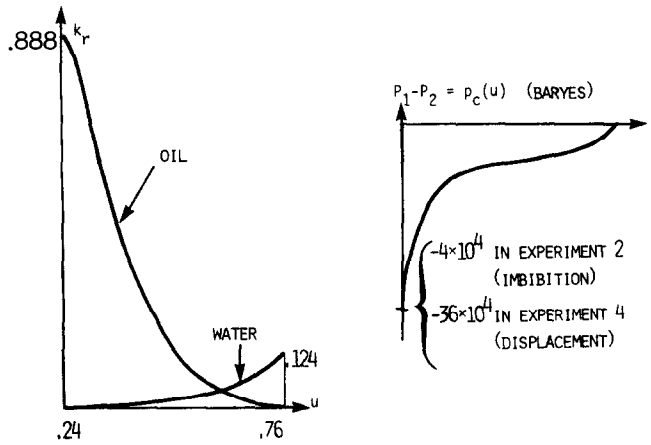

FIG. 8. The relative permeability and capillary pressure curves for the second set of laboratory data (water and oil).

(iii) the shape of $f(u)$, which depends on q and $\cos\gamma$. The two following combinations are used:

$$q = 0, \quad \cos\gamma = 0, \quad \text{and} \quad \cos\gamma = 1 \quad \text{(imbibition experiment)},$$
$$q(t) = 0.71 \times 10^{-5}\ \text{cm/s}, \quad \cos\gamma = 0 \quad \text{(displacement experiment)},$$

(iv) the boundary conditions, and

(v) the initial condition, given by (59).

The characteristics of each run are indicated hereon in by this scheme where the

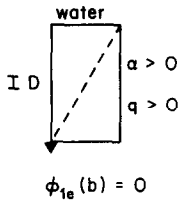

arrow indicates the choosen orientation of the x axis; "water" (resp. "oil" or "gas") indicates that the corresponding Dirichlet condition (in the sense of (12), if $\alpha \equiv 0$) is used; "$\phi_{1e}(b) = 0$" (resp. "$\phi_{1e}(b) = 2q$") indicates that a no-water or no-gas flow (resp. a no-oil flow) condition is used; "unilateral" indicates that a unilateral condition (U) is used, and --- indicates the initial condition; "ID" (resp. LD1 or

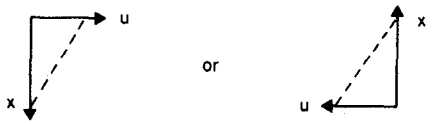

LD2) indicates that idealized (resp. laboratory) data are used; $\alpha > 0$ (resp. $\alpha = 0$) indicates that capillary pressure is taken into account (resp. neglected); and $q > 0$ (resp. $q = 0$) indicates that a displacement (resp. imbibition or segregation) experiment is being simulated.

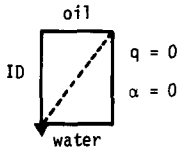

2. *Comparison Between the Finite-Difference Scheme* ($k = 0$) *and the Finite-Element Scheme* ($k = 1$) *on the Pure Transport Case for Idealized Data*

The analytical solution of the problem is shown at various times in Fig. 9. Due to the effects of gravity, the water which is in the top of the sample tends to descend, thus filling up the bottom. At time $t > 1.5$ one arrives at a stationary solution so that the top half of the sample is full of oil and the bottom half is full of water. There are no water flows through the lower and upper faces, as $\phi_1 = f(u) = u(1-u) = 0$ for $u = 0$ and $u = 1$.

The result obtained using a finite-element scheme, where one has $h = 0.1$ and $\Delta t = 0.05$, are most satisfactory. The computed solution at time $t = 0.75$ is shown in Fig. 10. Note that the discontinuities are well represented. The CPU time on a PDP11/40 is 1.4 s for each time step.

A finite-difference scheme has been applied to the same example, with *the same number of numerical unknowns* with $h = 0.05$ and $\Delta t = 0.05$. The solution obtained at time $t = 0.75$ is shown in Fig. 11. The discontinuities are more smeared than with the

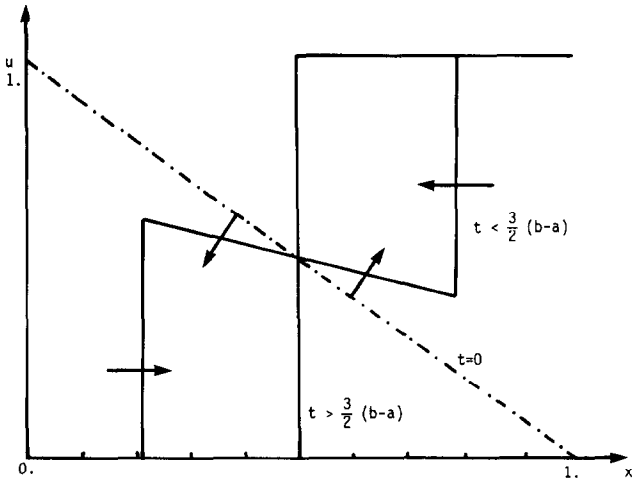

FIG. 9. Analytical solution.

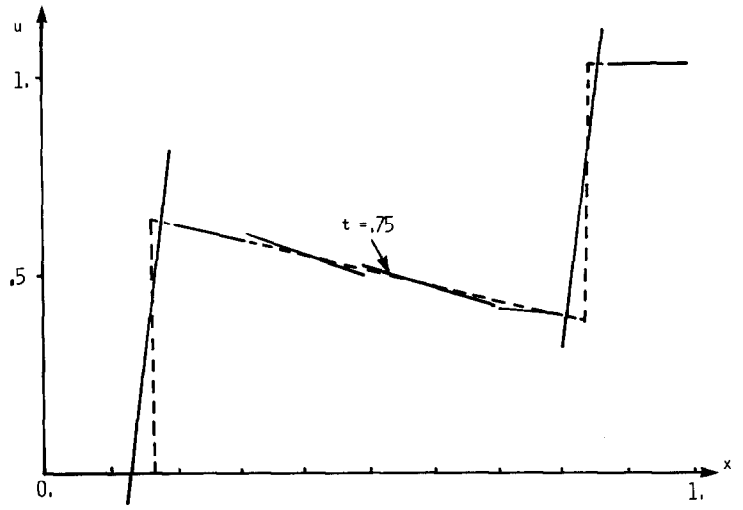

FIG. 10. Calculated solution by scheme with $k = 1$.

finite-element scheme. The CPU time for one time step is 1.09 s. To obtain as sharp a front as the finite-element method, it is necessary in the finite-difference scheme to take $h = 0.02$ and $\Delta t = 0.02$. The CPU time increases to 3.8 s for one time step (about three times the CPU time for one time step of the scheme with $k = 1$). Only a finite-element scheme shall be used hereafter.

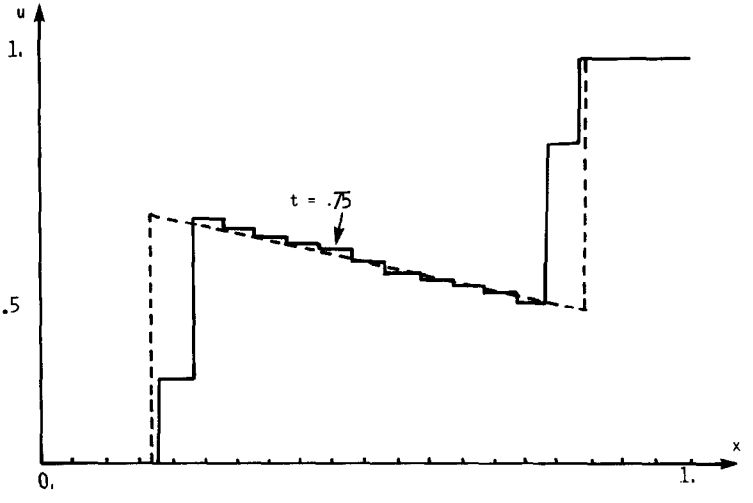

FIG. 11. Calculated solution by scheme with $k = 0$.

3. *Experiment* 1: *Segregation by Gravity*

In this experiment, we study the effect of gravity on two immiscible fluids of different densities contained in a vertical core sample insulated at both ends. The total flow $2q(t)$ of the two fluids is, necessarily, equal to zero, so that $f(u) = c(u)q_1$ is strongly nonmonotone (cf. (55) for ID case and Fig. 7 for the LD1 case). One analyzes this case with and without capillary pressure, and compares the obtained results both on idealized and laboratory data.

Case 1. Absence of capillary pressure ($\alpha = 0$).

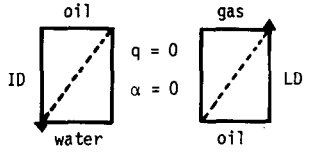

As in Section 2, $\alpha = 0$ requires generalized Dirichlet condition (12), and *so we cannot directly impose a no-water or no-gas flow* condition at the two extremities of the sample. So we have supposed that the sample was in contact at the top with the lighter fluid and at the bottom with the heavier fluid. This choice is justified by

Remark 9. As f is equal to $u(1-u)$ for the ID case or has the shape indicated at bottom left of Fig. 7 for the LD1 case, one can check that the computed Godunov values ξ_1^n and ξ_{I+1}^n at $x = a$ and $x = b$ are

$$\xi_1^n = u_e(a) = U_{\min} \qquad \text{as long as} \quad u_1^{+n} < U_{\max},$$
$$\xi_{I+1}^n = u_e(b) = U_{\min} \qquad \text{as long as} \quad u_{I+1}^{-n} > U_{\min},$$

so that the *computed water flow* satisfies (as practically, $u_{I+1}^{+n} \ll U_{\max}$ and $u_{I+1}^{-n} \gg U_{\min}$)

$$\phi_{1h}^n(a) = q(t) + f(\xi_1^n) = 0, \qquad \forall n,$$
$$\phi_{I+1}^n(b) = q(t) + f(\xi_{I+1}^n) = 0, \qquad \forall n.$$

This means that *when f has the above-mentioned shape and when the Dirichlet condition* (in the sense of (12)!) $u = U_{\min}$ *at* $x = a$ *and* $u = U_{\max}$ *at* $x = b$ are used, the *numerical solution behaves so as to exactly satisfy a no-water and no-oil flow condition* through the two extremities of the core sample. ∎

We now turn to the numerical results

Idealized data. This example was presented in Section 5.2. The calculated solution at time $t = 0.6$ s (—) as well as an asymptotic one are presented in Fig. 12 (···, $t = \infty$; ·-·, exact).

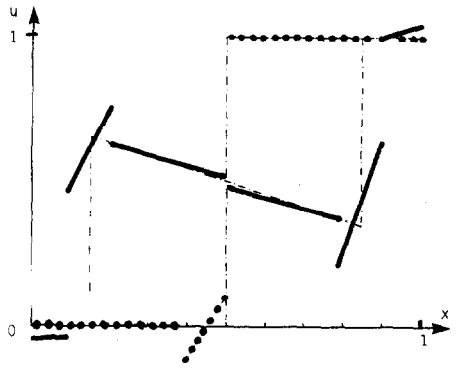

FIG. 12. Experiment 1, idealized data: water saturations ($\alpha \equiv 0$).

Laboratory data 1. The solution behaves in a similar way: the gas tends to accumulate at the top. Figure 13 shows the solution at times $t = 3200$ s (—), 6400 s (···), and 11,200 s (---).

Remark 10. As mentioned at the end of Section 3, the scheme (with $k = 1$) is nonmonotone, so that the computed saturation may not be bounded within $[U_{\min}, U_{\max}]$ (e.g., example near $x = 0$ and $x = 1$ in Fig. 12). ▮

Case 2. Presence of capillary pressure ($\alpha \neq 0$).

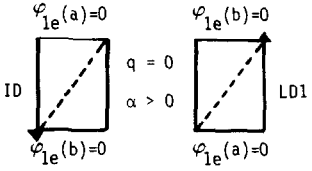

We can now use the no-flow boundary conditions.

FIG. 13. Experiment 1, first set of laboratory data: gas saturations ($\alpha = 0$).

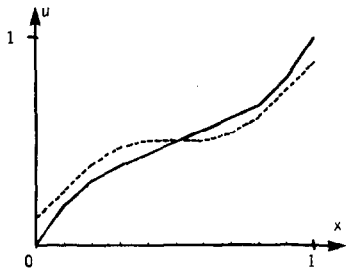

FIG. 14. Experiment 1, idealized data: water saturations ($\alpha \neq 0$).

Idealized data. The solution will not be discontinuous due to the effects of the capillary pressure, but is similar to Case 1. The water concentration at $x = a$ tends to zero, and at $x = b$ tends to one. The stationary solution is computed at $t = 6$ s. Figure 14 represents the solution at time $t = 0.6$ s (---) and its stationary configuration. A comparison between Figs. 12 and 14 is useful in analyzing the effects of diffusion.

Laboratory data 1. The observation made for the idealized data can be repeated in a similar way. The top portion fills up with gas, the oil accumulates at the bottom. The gas saturation at top ($x = b$) comes very close to, but does not quite reach, maximum saturation. The calculated solution at time $t = 3{,}200$ s (—) 11,200 s (---), and 20,800 s (·--·) is shown in Fig. 15.

Remark 11. If we denote by $u_\infty(t)$ the steady-state solution, given by

$$p_c(u_\infty(x)) - p_c(u_\infty(a)) = (\rho_1 - \rho_2)\, g(x - a) \cos \gamma \tag{61}$$

the shape of the saturation contour for large t tends to the shape of the capillary pressure curve (compare the contour $t = 20{,}800$ s and Fig. 6). ∎

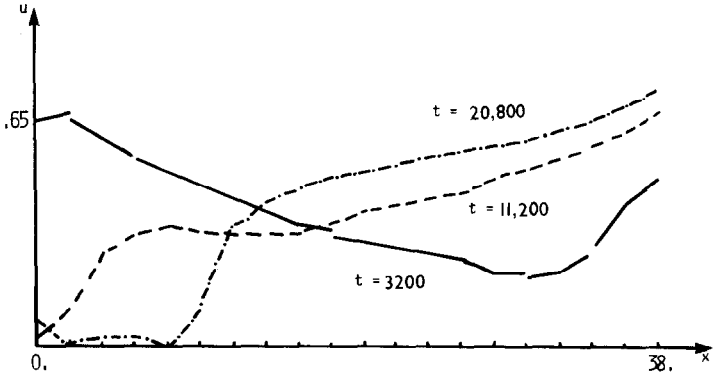

FIG. 15. Experiment 1, first set of laboratory data: gas saturations ($\alpha \neq 0$).

4. *Experiment* 2: *Imbibition With and Without Gravity*

In this experiment, we analyze the imbibition phenomenon, using the second set of laboratory data (water and oil) with and without gravity. Consider a core sample

Case 1. Horizontal sample.

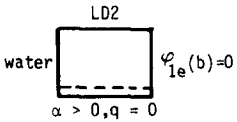

In this case, $f(u) \equiv 0$, a pure diffusion equation. Due to the effects of capillary pressure, the water enters the sample, and slowly advances toward $x = b$. The saturation contours after 120, 200, 280, 360, and 438 h are represented in Fig. 16. Figure 17 shows $(\varphi_1(a))$ the water flow or oil production rate through $x = a$ (mm^3/h) at various times.

Case 2. Vertical sample.

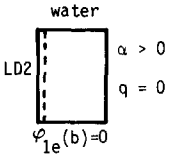

Now f is given at bottom left in Fig. 7. This case is interesting because of the importance of the effect of gravity. Once the water has penetrated the sample through the effect of capillary action, it comulates at the bottom of the sample through the effect of gravity (Fig. 18). Figure 20 shows the water saturation contours after 280 h with horizontal and vertical samples. Figure 19 shows $(\varphi_1(a))$ the water flow or oil production rate passing $x = a$ (mm^3/h) (cf. Fig. 17).

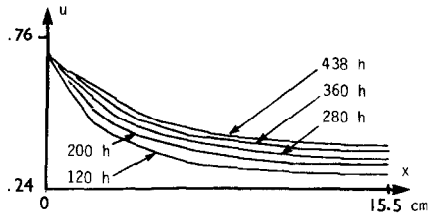

FIG. 16. Experiment 2, imbibition without gravity: water saturation contours.

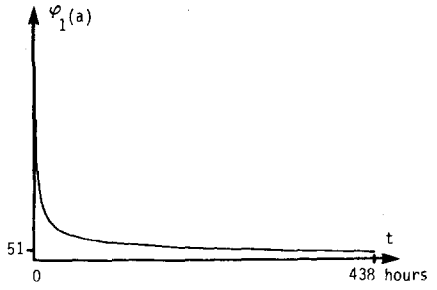

FIG. 17. Experiment 2, imbibition without gravity: oil production rate.

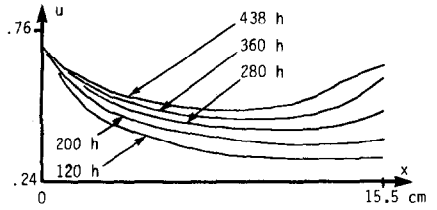

FIG. 18. Experiment 2, imbibition with gravity: water saturation contours.

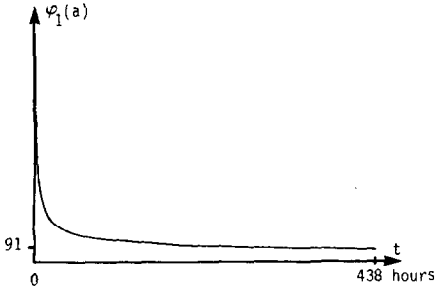

FIG. 19. Experiment 2, imbibition with gravity: oil production rate.

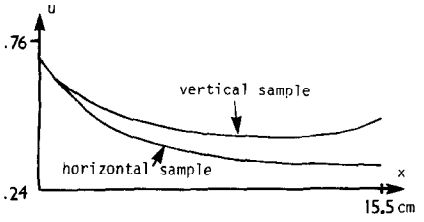

FIG. 20. Experiment 2, comparison between imbibition with and without gravity.

5. *Experiment* 3: *Permanent Counterflows*

This experiment is concerned with counterflows in a sample with the top in contact with the heavier fluid and the bottom with the lighter one. We shall investigate two cases with and without capillary pressure, using both the idealized data and the first set of laboratory data (gas and oil).

Case 1. No capillary pressure.

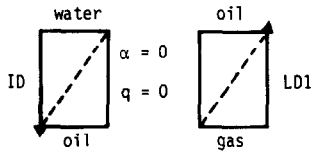

Runs on idealized data ($f(u) = u(1-u)$). The analytical solution of this problem is known, as shown in Fig. 21 (---, $t = 0$; $\cdots$, $t = \infty$). The water at the top of the sample tends to descend. This creates counterflows so that there is displacement of the oil which tends to rise. The solution tends to a steady state where water and oil are simultaneously present and flowing in opposite directions. In Fig. 22, the obtained solution at times $t = 0.4$ (—) and $t = 2$ s (---) is compared with that shown in Fig. 21.

Runs on laboratory data 1. The solution is similar to the runs on idealized data. In Fig. 23, we show the computed solution at times $t = 3200$ s (—) and 11,200 s (---).

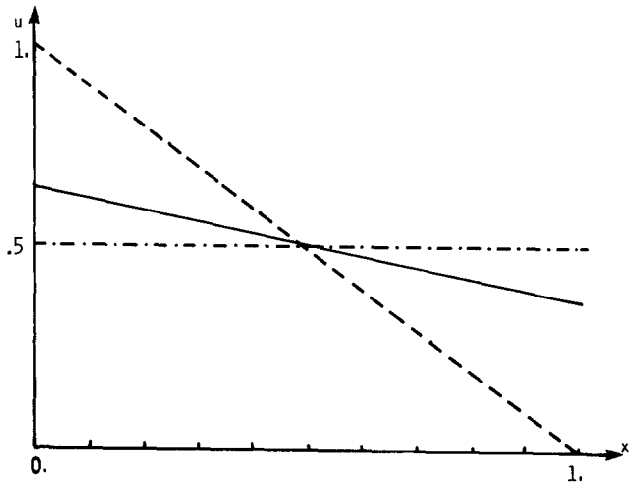

FIG. 21. Experiment 3, idealized data: analytical solution ($\alpha = 0$).

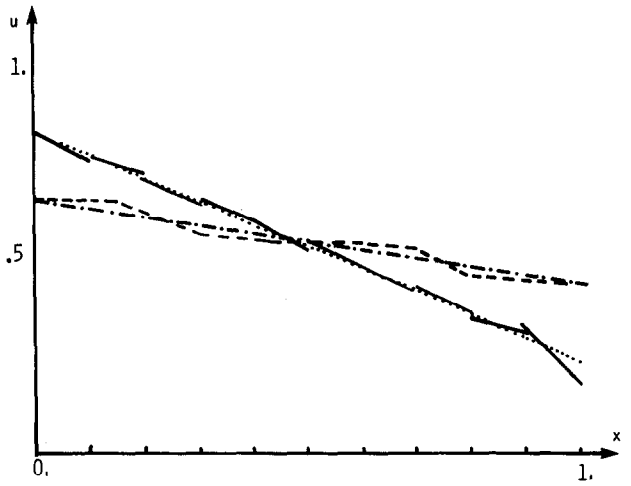

FIG. 22. Experiment 3, idealized data ($\alpha = 0$): water saturation.

Case 2. Presence of capillary pressure.

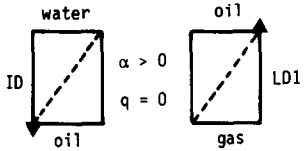

Figure 24 shows the saturation contours at times $t = 0.4$ s (—) and 2 s (- - -). These curves are very close to the steady state solution (cf. Remark 11). There are permanent counterflows of oil and water through the upper and lower end of the

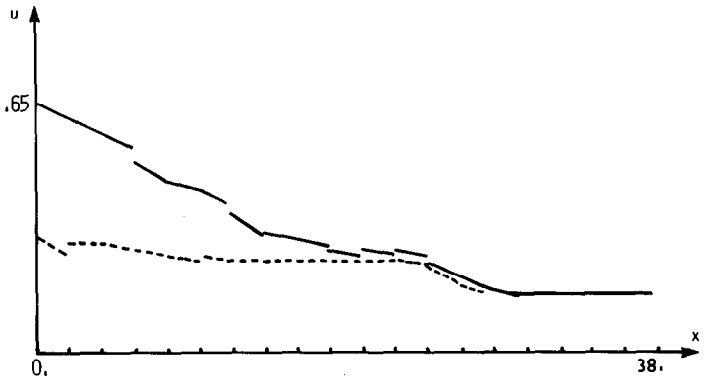

FIG. 23. Experiment 3, laboratory data 1, ($\alpha = 0$): gas saturation.

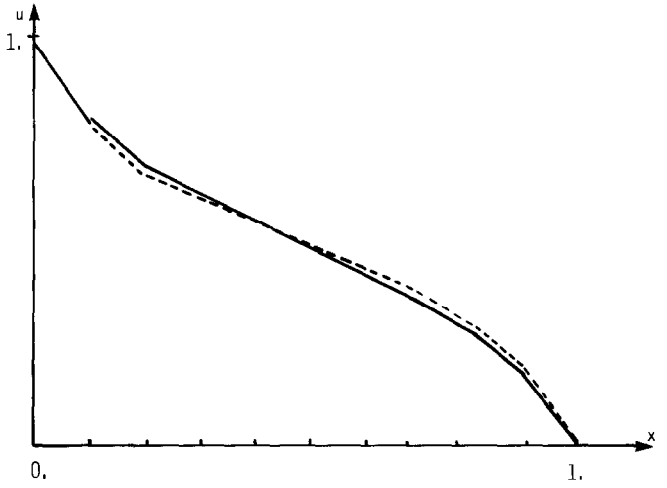

FIG. 24. Experiment 3, idealized data: counter flows ($\alpha = 0$).

sample: *on the upper end,* $u = 1$ implies $p_c = 0$, *and the* (PCR) *is satisfied; on the lower end,* $u = 0$ implies $p_c < 0$ *so that the* (PCR) *is not satisfied.*

Runs on laboratory data 1. Figure 25 shows the computed solution at times $t = 3200$ s (—) and 11,200 s (---). Compare with Fig. 23 in order to analyze the effects of diffusion especially at the extremities. In this case, as gas is the nonwetting fluid, the (PCR) is satisfied at the upper end $x = b$ but not at the lower end $x = a$.

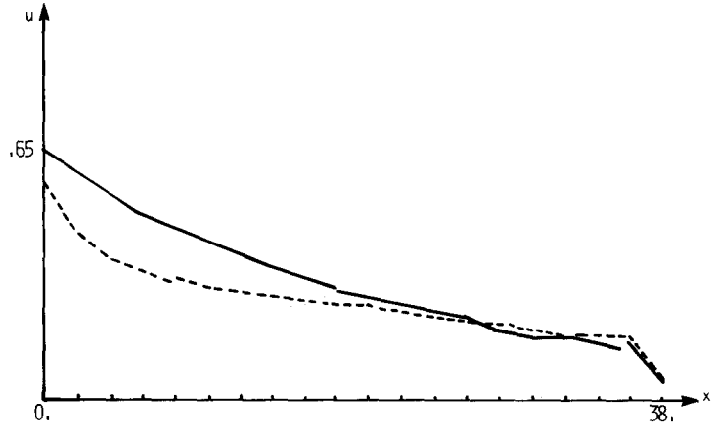

FIG. 25. Experiment 3, laboratory data: counter flows ($\alpha > 0$).

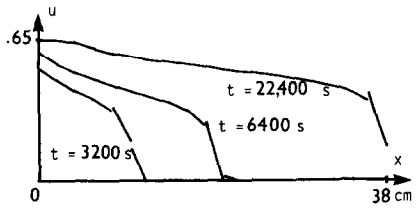

FIG. 26. Experiment 4, gas injection through the top: gas saturations.

6. *Experiment* 4: *Displacements of Oil by Gas or Water* (laboratory data)

This is the most interesting experiment from the point of view of the simulation and practical utilization of the results. The oil trapped in the sample is recovered through injection of gas or water through the $x = a$ extremity. We shall first simulate gas injection in a vertical or horizontal sample to illustrate the ability of the algorithm to take care of gravity and to track sharp fronts, and secondly, simulate water injection in a horizontal sample in order to illustrate the effect of the unilateral condition.

For all runs, we have $\alpha > 0$, $q > 0$, *a given gas or water injection rate condition at* $x = a$ *and the unilateral condition at* $x = b$.

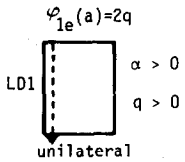

Gas injection through the top ($f(u)$ given at top right of Fig. 7). The injected gas penetrates the sample and the gravity tends to retain it toward the top, yielding sharp fronts. The gas breakthrough is obtained after 12,432 s (≃3 h 27 min). Figure 26 shows the solutions calculated at times $t = 3200$ s, $t = 6400$ s, and $t = 22{,}400$ s.

The accumulation of the wetting phase (here oil) against the production end $x = b$ caused by the unilateral condition ("well effect") appears in Fig. 26 clearly. As we mentioned earlier, the unilateral condition for gas injection reduces to the Dirichlet condition $u = u_p = U_{\min} = 0$. The gas flow through $x = b$ appears in Fig. 30.

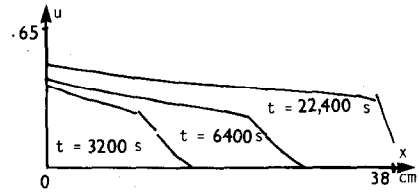

FIG. 27. Experiment 4, gas injection without gravity: gas saturations.

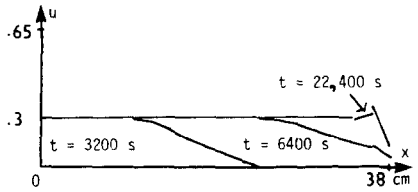

FIG. 28. Experiment 4, gas injection through the bottom: gas saturations.

Gas injection without gravity ($f(u)$ given at middle right of Fig. 7). In this case the gas break through occurs after 8460s ($\simeq$2 h 21 min), i.e., approximately 1 hour earlier than when gas is injected through the top. The gas saturation at the injection end does not attain its maximum value. The gas saturation contours are shown on Fig. 27, and the gas flow through $x = b$ on Fig. 30.

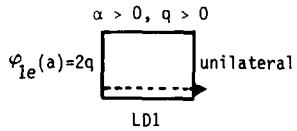

Gas injection through the bottom ($f(u)$ given at bottom right of Fig. 7). Now (cf. Fig. 28) the transport and gravity forces act in the same direction and the gas arrives very quickly at the production end (the breakthrough already occurs after 5088 s, i.e., 1 h 14 min) and does not displace all of the oil contained in the sample (the maximum gas saturation attained during the experiment corresponds exactly to the saturation value which maximizes $f(u)$). The gas flow through $x = b$ is shown in Fig. 30.

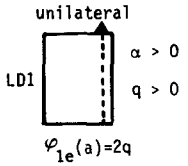

We now turn to the experiments where water displaces oil, using the second set of laboratory data.

Water injection without gravity: The effect of the unilateral condition. We have shown in Fig. 31 a few saturation contours around the breakthrough time. For every

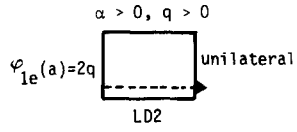

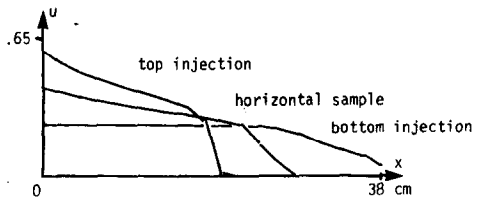

FIG. 29. Experiment 4, influence of gravity on the gas saturation countours after 6400 s.

time $t^n = n\,\Delta t$, we have drawn in Fig. 31 both the function u_h^n defined in (33) and the two numbers (u_a^n, u_b^n) defined in (34) and representing the approximation of the trace of $u(\cdot, t)$ at $x = a$ and $x = b$.

The effect of the unilateral condition appears in Fig. 31 clearly: as the water arrives at the production end $x = b$, it first accumulates there until the boundary saturation u_b^n reaches the maximum saturation $U_{\max}$ (for which the capillary pressure vanishes). The breakthrough time is then defined as the first time this occurs (here, 4144 min). After the breakthrough time, the boundary saturation u_b^n stays at its maximum value and water starts to be produced simultaneously with oil.

This appears contradictory at first, as the oil filtration velocity through $x = b$ is given, after the breakthrough time, by (cf. (4), (5), (8), where $q_1 = 0$ and $b(U_{\max}) = 1$),

$$\varphi_2(b, t) = K\alpha'(u_{\max})\frac{\partial u}{\partial x}(b, t), \tag{60}$$

where $\alpha'(u_{\max}) = [k_1(u_{\max})\,k_2(u_{\max})/(k_1(u_{\max}) + k_2(u_{\max}))](dp_c/du)\,(u_{\max})$ generally vanishes together with $k_2(u_{\max})$, so that $\varphi_2(b, t)$ should seemingly be equal to zero. This is not true, as we know from the experiments, and can be explained by the fact that the saturation derivative $(\partial u/\partial x)(b, t)$ is infinite, which corresponds to the

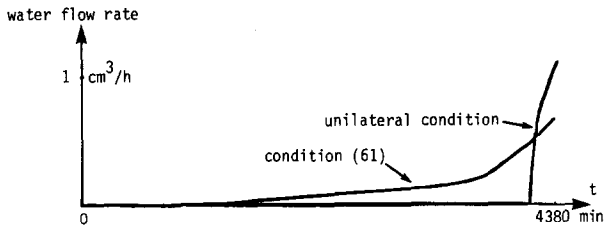

FIG. 33. Water production rate through $x = b$ with two types of boundary conditions (the water injection rate is 2.31 cm^3/h).

condition and condition (61) tends to zero under those conditions. So the unilateral condition can be seen as an extension of condition (61) which remains valid for slow displacements with capillary pressure. ∎

7. CPU *Times*

The runs have been made on a digital PDP11/40. In all the runs on realistic data, one has take $h = 2$ cm. Different CPU times were recorded for various boundary conditions. For example, for experiment 1 and Dirichlet boundary condition at $x = a$ and $x = b$, the CPU time for one time step is 2.36 s. For experiment 4 with two Neumann boundary conditions, the CPU time for one time step is equal to 3.4 s.

6. CONCLUSIONS

An approximation of a one-dimensional *quasilinear-diffusion/transport equation* using finite elements is presented. It reduces to the well-established technique of Lesaint's discontinuous-finite elements (resp. Thomas's mixed elements) in the limiting case of a pure transport equation (resp. a pure diffusion equation). Boundary conditions well suited to the simulation of 1-D water flooding are incorporated. The gravitational effects, leading to a nonmonotone transport term, are taken into account.

Numerical simulation of 1-D two-phase flows under various conditions (ranging from pure diffusion to pure transport cases, including strongly nonmonotone fractional flow curves and comparisons with exact solutions when available) are presented, and shown to give satisfactory results.

Work is in progress on the solution of the corresponding inverse problem (cf. Cohen [14, 17]) and the extension of the above approximation techniques to the two-dimensional case (cf. Jaffré [15, 16]).

APPENDIX: NOTATION

$\blacksquare$ the end of a logical unit (Remark, paragraph, etc.)

$\Omega = (a, b)$ spatial domain, with boundary $\Gamma = \{a, b\}$

σ cross-sectional area of core sample

T duration of experiment

x, t space and time coordinates

Φ, K porosity, absolute permeability of core sample

g gravity acceleration

$u(x, t)$ reduced water saturation at point x and time t in Sections 1–4, $0 \leqslant u(x, t) \leqslant 1$; actual saturation in Section 5—numerical results, $U_{\min} \leqslant u(x, t) \leqslant U_{\max}$

u_P value of saturation for which capillary pressure vanishes (typically $u_P = 1$ if u is the wetting phase saturation)

$u_0(x)$ given initial water saturation distribution

u_a, u_b trace of u on $\Gamma = \{a, b\}$

$u_e(a), u_e(b)$ given Dirichlet data for the saturations on Γ

$q(t)$ half (oil + water) filtration velocity at time t (independent of x)

ρ_j, μ_j density and viscosity
$k_{jr}(u)$ relative permeability curve
$k_j(u) = k_{jr}(u)/\mu_j$ mobility
} of the jth fluid with $j = 1$ for water and $j = 2$ for oil

$d(u) = k_1(u) + k_2(u)$

$\rho(u) = (\rho_1 k_1(u) + \rho_2 k_2(u))/d(u)$

$p_c(u) = P_1 - P_2$ capillarity pressure curve

$$\rho(u) = \int_0^u \frac{dp_c}{du}(v) \frac{k_1(v)\, k_2(v)}{d(v)}\, dv$$ nonlinearity in the diffusion term

$b(u) = (k_1(u) - k_2(u))/d(u)$

$c(u) = (\rho_1 - \rho_2)\, k_1(u)\, k_2(u)/d(u)$

$\cos\gamma$ cosine of the angle of the x axis with the vertical direction oriented toward the bottom

$q_1 = Kg \cos\gamma$

$f(u, t) = q(t)\, b(u) + q_1 c(u)$ nonlinearity in the transport term

$\phi_1(x, t)$ water filtration velocity at point x and time t

$\phi_2(x, t)$ oil filtration velocity at point x and time t

ϕ_{1a}, ϕ_{1b} trace of ϕ_1 on $\Gamma = \{a, b\}$

$\phi_{1e}(a), \phi_{1e}(b)$ given Neumann data for water filtration velocities ϕ_1 on Γ

$$r(x, t) = -K \frac{\partial}{\partial x} \alpha(u)$$ half (water–oil) filtration velocity caused by capillary diffusion

$\operatorname{sg}(\xi) = +1$ if $\xi > 0$, $=0$ if $\xi = 0$, $=-1$ if $\xi < 0$ (sign function),

$I(\alpha, \beta) = (\min(\alpha, \beta), \max(\alpha, \beta))$

$I[\alpha, \beta] = [\min(\alpha, \beta), \max(\alpha, \beta)]$

$\nu_s = +1$ for $s = b$,
$= -1$ for $s = a$,
} = cosine of the "normal" to Ω with the x axis

$V(\alpha,\beta)=\dfrac{f(\alpha)-f(\beta)}{\alpha-\beta}$ Rankine–Hugoniot speed of propagation of a discontinuity jumping from the value α to the value β

$a=x_1<x_2<\cdots<x_{I+1}=b$ space discretization

$h=(b-a)/I=x_{i+1}-x_i$ space step for a regular mesh

$0=t^1<t^2<\cdots<t^{N+1}=T$ time discretization

$\Delta t=t^{n+1}-t^n$ time increment, constant

$\mathscr{P}^k$ space of polynomials of degree less or equal to k in the variable x

$V_h\subset L^2(\Omega)$ finite-dimensional space for the approximation of $u(\cdot,t)$

$u_h^n\in V_h$ approximation (in the L^2 sense) of $u(\cdot,t)$ in V_h

u_a^n, u_b^n approximation of the traces $u(a,t^n)$, $u(b,t^n)$ of u on Γ when they exist, i.e., when diffusion is present

u_i^{+n}, u_i^{-n} right- and left-hand values of u_h^n at x_i, $i=1,2,\ldots,I+1$, with the conventions

$u_1^{-n}=u_e(a)$ Dirichlet data for $\alpha\equiv 0$,
u_a^n approximation of the trace of u for $\alpha\not\equiv 0$,

$u_{I+1}^{+n}=u_e(b)$ Dirichlet data for $\alpha\equiv 0$,
u_b^n approximation of the trace of n for $\alpha\not\equiv 0$

$u_{i+1/2}^n=u_h^n((x_i+x_{i+1})/2)$,

$Q_h\subset\mathscr{C}^0(\Omega)$ finite-dimensional space for the approximation of $r(\cdot,t)$

$r_h^n\in Q_h$ approximation of $r(\cdot,t)$

$r_i^n=r_h^n(x_i)$, $i=1,2,\ldots,I+1$

$r_{i+1/2}^n=r_h^n((x_i+x_{i+1})/2)$, $i=1,2,\ldots,I$

$\{\ \}$ a set

REFERENCES

1. C. L. BARDOS, A. Y. LEROUX, AND J. C. NEDELEC, *Rapp. Interne CMA* **38** (1978).
2. P. A. RAVIART AND J. M. THOMAS, "A Mixed Finite Element Method for Second Order Elliptic Problem," Lecture Notes in Mathematics, Vol. 606, Springer Pub., New York, 1977.
3. P. LESAINT AND P. A. RAVIART, *in* Symposium on Mathematics, Aspects of Finite Elements in PDE, Mathematics Research Center, Univ. of Wisconsin, Madison, 1974.
4. S. K. GODUNOV, *Mat. Sb.* **47** (3) (1959), 271.
5. G. CHAVENT, "About the Identification and Modelling of Miscible or Immiscible Displacement in Porous Media," Lecture Notes in Control and Information Science, Vol. 1, Springer Pub., New York, 1978.
6. G. CHAVENT AND G. COHEN, *in* "Lecture Notes in Control and Information Science," Vol. 6, Springer Pub., New York, 1978.
7. G. SALZANO, *Rapp. INRIA* **2** (1980).
8. C. MARLE, "Cours de Production," Vol. IV, Technip, 1965.
9. G. CHAVENT, *in* "Lecture Notes in Mathematics," Vol. 503, Springer Pub., New York, 1976.
10. G. CHAVENT, *Rapp. Lab.* **260** (1977).
11. G. GAGNEUX, *J. Méc.* **19** (2) (1980), 1–31.
12. A. Y. LEROUX, "Approximation de Quelques Problèmes Hyperbolique Nonlinéaires," Thèse d'État, Rennes, France, 1979.

13. B. VAN LEER, *J. Comput. Phys.* **23** (3) (1977), 276–299.
14. G. COHEN, "Résolution Numérique et Identification pour une Équation Quasiparabolique Non Linéaire Dégénérée de Diffusion et Transport en Dimension Un," Thèse de 3ème cycle, 1978.
15. J. JAFFRÉ, *in Comput. Fluids* **8** (1980), 177–188.
16. J. JAFFRÉ, *Rapp. INRIA* **37** (1980).
17. G. COHEN, G. CHAVENT, AND M. ESPY, *in* "55th Annual Fall Technical Conference and Exhibition of the Society of Petroleum Engineers of AIME, Dallas, Texas," September 12–24, 1980.